Numerical Heat Transfer, Part A, 36:473–488, 1999

1040–7782 /99 $12.00 + .00

NATURAL CONVECTION PHENOMENA AFFECTED BY RADIATION IN CONCENTRIC AND ECCENTRIC HORIZONTAL CYLINDRICAL ANNULI

Cho Young Han and Seung Wook Baek
Department of Aerospace Engineering, Korea Advanced Institute of Science and Technology, 373-1 Kusong-dong, Yusong-ku, Taejon 305-701, Korea

A numerical investigation has been performed to study the radiation-affected steady-laminar natural convection induced by a hot inner cylinder under a large temperature difference in the cylindrical annuli filled with a gray gas. To examine the effects of thermal radiation on thermofluid dynamics behavior in the eccentric geometry, the generalized body-fitted coordinate system is introduced while the finite volume method is used for solving the radiative transport equation. After validating numerical results for the case without radiation, the detailed radiation effect is discussed. Based on the results of this study, when there exists a large temperature difference between two cylinders, the existence of a radiatively participating medium is found to incur a distinct difference in fluid dynamics as well as thermal behavior.

INTRODUCTION

Although phenomena of natural convection have been investigated by many researchers, the interaction between natural convection and radiation in participating media still remains as an important problem in the development of fluid dynamic and thermal processes related to various engineering systems. In these types of problems, the momentum and energy equations are inherently coupled one another through the transfer equation governing the radiative intensity.

In the last decade, numerous numerical methods have been proposed to solve the radiative transfer equation (RTE). Among them is the discrete ordinates method (DOM) [1], which is a kind of multiflux method. Han and Baek [2] have already adopted this technique to analyze ignition phenomena over the vertical fuel plate due to thermal radiation. However, the application of DOM to a complex geometry using the general body-fitted coordinate system is formidable. Thereby, Chui and Raithby [3] and Chai et al. [4] recently proposed the finite volume method (FVM) for overcoming these difficulties. This method has been successfully applied to various problems in radiative equilibrium, proving its accuracy in the nonorthogonal as well as orthogonal coordinate systems. Kim and Baek [5] have also adopted FVM to examine combined heat transfer in a gradually expanding channel, showing that it is compatible with flow solvers, also based on the finite volume method. Whereas FVM is very similar to DOM in many ways, it

Received 10 February 1999; accepted 23 April 1999.
Address correspondence to Professor Seung Wook Baek, Department of Aerospace Engineering, Korea Advanced Institute of Science and Technology, 373-1 Kusong-dong, Yusong-ku, Taejon 305-701, Korea. E-mail: swbaek@sorak.kaist.ac.kr

NOMENCLATURE

A	surface area for heat transfer	x, y	Cartesian coordinates
C_p	specific heat at constant pressure, J/(kg K)	β	extinction coefficient, 1/m
		δ	overheat ratio $[= (T_H - T_C)/T_0]$
D	diameter of cylinder, m	ε	emissivity
e_v	vertical eccentricity	θ	polar angle, rad
Fr	Froude number $[= u_0/(gL)^{1/2}]$	κ_a	absorption coefficient, 1/m
g	gravitational acceleration, m/s^2	μ	viscosity, kg/(m s)
Gr	Grashof number $[= g\beta_0 \rho_0^2 L^2 (T_H - T_C)/\mu_0^2$, where $\beta = 1/T$ for ideal gas]	ξ, η	axes of curvilinear coordinates
		ρ	density, kg/m^3
		σ	Stefan-Boltzmann constant $[= 5.67 \times 10^{-8}$ W/(m^2 K^4)]
I	radiation intensity, W/(m^2 Sr)		
k	thermal conductivity, W/(m K)	σ_s	scattering coefficient, 1/m
L	reference length $[= (D_o - D_i)/2]$, m	τ	optical thickness $(= \beta L)$
		ϕ	azimuthal angle, rad
$\hat{n}$	unit normal vector	Φ	scattering phase function, 1/sr
N	conduction to radiation parameter $[= k_0 \beta_0/(4\sigma T_0^3)]$	ω	scattering albedo
		Ω	solid angle, sr
Nu	Nusselt number $[= \dot{q}_w'' L/(k_0 \delta T_0)]$		
p	pressure, N/m^2	**Subscripts**	
Pr	Prandtl number $(= C_{p0} \mu_0/k_0)$		
q	local heat flux	e, w, n, s	east, west, north, and south faces of a control volume
Q	overall heat transfer from the surface	E, W, N, S	east, west, north, and south neighbors of the grid point P
$\mathbf{r}$	position vector		
R	distance from center of inner cylinder to outer cylinder	i	inner
		o	outer
Re	Reynolds number $(= \rho_0 u_0 L/\mu_0)$	P	pertaining to the grid point P
s	distance traveled by ray	w	wall
$\hat{s}$	unit direction vector	0	reference quantities
S	source term		
T	temperature, K		
T_C, T_H	cooled and heated cylindrical wall temperature, K	**Superscripts**	
T_0	reference temperature $[= (T_H + T_C)/2]$, K	C	conduction
		R	radiation
u_0	reference velocity $[= (gL\delta)^{1/2}]$	T	total quantity
u, v	velocity components in x and y directions, m/s	*	dimensionless quantities
		′	incoming direction

has its own flexibility in assigning the directional rays so that the directional weights are accordingly determined, as opposed to DOM, in which the angular directions are reserved following a strict constraint. Since there is no limitation to the selection of control angles with FVM, it can easily be applied to the generalized body-fitted coordinate system.

Regarding the natural convection between horizontal concentric and eccentric cylinders, Kuehn and Goldstein [6, 7] have extensively performed experimental and theoretical works, while Cho et al. [8] examined it numerically. However, they assumed that only a small temperature difference was involved in the problem; the

Boussinesq approximation has been utilized, neglecting the density variation as well as radiation heat transfer. A problem of natural convection with radiation effect was investigated by Lauriat [9] for a rectangular cavity. But the density variation due to significant temperature change was neglected in the medium. Fusegi and Farouk [10] also conducted a numerical work in the rectangular cavity, in which the participating medium was assumed to be nongray with the overheat ratio of unity. But the generalized body-fitted coordinate was not used in their calculation.

For this study we consider the natural convection phenomenon induced by a large temperature difference in the horizontal cylindrical annuli positioned either concentrically or eccentrically. Its applications reside in the solar collector design, melting of a phase change material around a heating pipe in a thermal storage system, electric transmission cables, and heat transfer phenomena around nuclear fuel bundles in a nuclear reactor.

The main objective of this investigation consists of examining the effects of thermal radiation on thermofluid dynamics behavior in the geometry aforementioned by introducing the generalized body-fitted coordinate system. FVM is used to solve the radiation transport because of the ease in handling the eccentric geometry. After confirming the numerical results without radiation, the radiation effect has been considered in detail by applying the FVM, which has not been done before.

THEORETICAL MODEL

A schematic of the eccentrically positioned cylindrical annulus, which is assumed to be filled with a gray gas, is shown in Figure 1. While the temperature of the outer cold cylinder with diameter D_o is held at T_C, that of the inner cylinder with diameter D_i is maintained at T_H. The eccentricity of the inner cylinder is denoted by the distance e_v. For convenience of the analysis, only a vertical eccentricity is considered here, so that only one-half of the physical domain is taken as a computational domain. The diameter ratio of cylinders (D_o/D_i) is fixed at 2.6, following Kuehn and Goldstein [7]. In order to analyze the combined heat

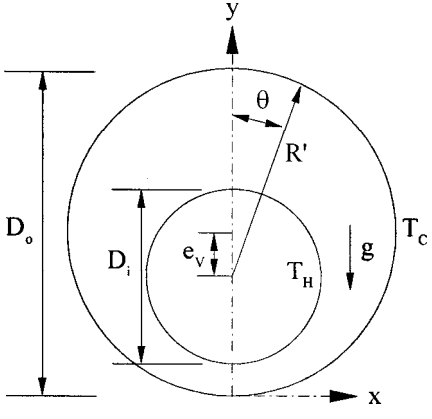

Figure 1. Eccentric annular cross section.

transfer of laminar flow, the following assumptions were made to simplify the problem:

1. The flow is steady and has constant properties.
2. Viscous work is negligible.
3. The gray gas absorbs, emits, and scatters radiation isotropically.
4. The wall surface is diffuse and isothermal.

Governing Equations

Since a very large temperature difference is involved in the current study, the Boussinesq assumption may not be applied so that the ideal gas equation is adopted. The governing equations are nondimensionalized using the following variables:

$$x^* = x/L \qquad y^* = y/L \qquad u^* = u/u_0 \qquad v^* = v/u_0 \tag{1}$$

$$p^* = \frac{p - p_0}{\rho_0 u_0^2} \qquad \rho^* = \rho/\rho_0 \qquad \mu^* = \mu/\mu_0 \qquad k^* = k/k_0 \qquad T^* = T/T_0 \tag{2}$$

$$\beta_0 = \kappa_{a0} + \sigma_{s0} \qquad \omega_0 = \sigma_{s0}/\beta_0 \qquad \tau_0 = \beta_0 L \qquad I^* = \frac{I}{\sigma T_0^4} \tag{3}$$

$$\mathrm{Fr} = \frac{u_0}{\sqrt{gL}} \qquad \mathrm{Pr} = \frac{C_{p0}\mu_0}{k_0} \qquad \mathrm{Re} = \frac{\rho_0 u_0 L}{\mu_0} \qquad N = \frac{k_0 \beta_0}{4\sigma T_0^3} \qquad \delta = \frac{T_\mathrm{H} - T_\mathrm{C}}{T_0} \tag{4}$$

The characteristic length L is defined as the difference in the cylinder radii, i.e., $L = (D_\mathrm{o} - D_\mathrm{i})/2$. The reference velocity is selected as $\mu_0 = (gL\delta)^{1/2}$ to relate Reynolds and Grashof numbers as follows: $\mathrm{Re}^2 = \mathrm{Gr}$ [10]. The overheat ratio is denoted by δ. The reference temperature is the arithmetic average of the two isothermal cylinder temperatures, i.e., $T_0 = (T_\mathrm{H} + T_\mathrm{C})/2$. The reference fluid properties are set equal to those of air at the reference temperature and presented in Table 1. For simplicity, the fluid properties are assumed to be constant except for the density. Based on the presumptions above, the dimensionless governing equations can be shown as follows:

Continuity

$$\frac{\partial}{\partial x^*}(\rho^* u^*) + \frac{\partial}{\partial y^*}(\rho^* v^*) = 0 \tag{5}$$

Table 1. Physical properties used in the study

T_0, K	p_0, N/m^2	C_{p0}, J/(kg K)	k_0, W/(m K)	μ_0 (N s)/m^2	ρ_0, kg/m^3
300	1.013×10^5	1.007×10^3	26.3×10^{-3}	184.6×10^{-7}	1.1614
600	1.013×10^5	1.051×10^3	46.9×10^{-3}	305.8×10^{-7}	0.5804

Momentum

$$\frac{\partial}{\partial x^*}(\rho^* u^{*2}) + \frac{\partial}{\partial y^*}(\rho^* u^* v^*) = -\frac{\partial p^*}{\partial x^*} + \frac{1}{\mathrm{Re}}\left[\frac{\partial}{\partial x^*}\left(\mu^* \frac{\partial u^*}{\partial x^*}\right) + \frac{\partial}{\partial y^*}\left(\mu^* \frac{\partial u^*}{\partial y^*}\right)\right] + S_u^*$$

where

$$S_u^* = \frac{1}{\mathrm{Re}}\left[\frac{1}{3}\frac{\partial}{\partial x^*}\left(\mu^* \frac{\partial u^*}{\partial x^*}\right) - \frac{2}{3}\frac{\partial}{\partial x^*}\left(\mu^* \frac{\partial v^*}{\partial y^*}\right) + \frac{\partial}{\partial y^*}\left(\mu^* \frac{\partial v^*}{\partial x^*}\right)\right] \tag{6}$$

$$\frac{\partial}{\partial x^*}(\rho^* u^* v^*) + \frac{\partial}{\partial y^*}(\rho^* v^{*2}) = -\frac{\partial p^*}{\partial y^*} + \frac{1}{\mathrm{Re}}\left[\frac{\partial}{\partial x^*}\left(\mu^* \frac{\partial v^*}{\partial x^*}\right) + \frac{\partial}{\partial y^*}\left(\mu^* \frac{\partial v^*}{\partial y^*}\right)\right] - \frac{1}{Fr^2}(\rho^* - 1) + S_v^*$$

where

$$S_v^* = \frac{1}{\mathrm{Re}}\left[\frac{1}{3}\frac{\partial}{\partial y^*}\left(\mu^* \frac{\partial v^*}{\partial y^*}\right) - \frac{2}{3}\frac{\partial}{\partial y^*}\left(\mu^* \frac{\partial u^*}{\partial x^*}\right) + \frac{\partial}{\partial x^*}\left(\mu^* \frac{\partial u^*}{\partial y^*}\right)\right] \tag{7}$$

Energy

$$\frac{\partial}{\partial x^*}(\rho^* u^* T^*) + \frac{\partial}{\partial y^*}(\rho^* v^* T^*) = \frac{1}{\mathrm{Re\,Pr}}\left[\frac{\partial}{\partial x^*}\left(\frac{k^*}{C_p^*}\frac{\partial T^*}{\partial x^*}\right) + \frac{\partial}{\partial y^*}\left(\frac{k^*}{C_p^*}\frac{\partial T^*}{\partial y^*}\right)\right] - \frac{1}{\mathrm{Re\,Pr}}\frac{\tau_0^2}{N}(1-\omega_0)\frac{1}{C_p^*}\left(T^{*4} - \frac{1}{4}\int_{4\pi} I^*\, d\Omega\right) \tag{8}$$

Equation of state

$$\rho^* = \frac{\rho_0 u_0^2}{p_0}\frac{p^*}{T^*} + \frac{1}{T^*} \tag{9}$$

Radiative transfer

$$\frac{1}{\tau_0}\frac{dI^*(\mathbf{r},\hat{\mathbf{s}})}{ds^*} = \frac{(1-\omega_0)}{\pi} T^{*4}(\mathbf{r}) - I^*(\mathbf{r},\hat{\mathbf{s}}) + \frac{\omega_0}{4\pi}\int_{4\pi} I^*(\mathbf{r},\hat{\mathbf{s}}')\Phi(\hat{\mathbf{s}}',\hat{\mathbf{s}})\, d\Omega' \tag{10}$$

In Eq. (10), $\Phi(\hat{\mathbf{s}}', \hat{\mathbf{s}})$ designates the scattering phase function of energy transfer from the incoming direction to the outgoing direction. Below, the superscript asterisk is dropped for convenience.

Boundary Conditions

The boundary conditions for diffusively reflecting and emitting isothermal walls are as follows

Inner wall

$$u = v = 0 \qquad T = 1 + \delta/2 \tag{11}$$

Outer wall

$$u = v = 0 \qquad T = 1 - \delta/2 \tag{12}$$

Both walls

$$I(\mathbf{r}_w, \hat{\mathbf{s}}) = \frac{\varepsilon_w(\mathbf{r}_w) T^4(\mathbf{r}_w)}{\pi} + \frac{1 - \varepsilon_w(\mathbf{r}_w)}{\pi} \int_{\hat{\mathbf{s}}' \cdot \hat{\mathbf{n}}_w < 0} I(\mathbf{r}_w, \hat{\mathbf{s}}') |\hat{\mathbf{s}}' \cdot \hat{\mathbf{n}}_w| \, d\Omega' \tag{13}$$

where $\varepsilon_w(\mathbf{r}_w)$ and $\hat{\mathbf{n}}_w$ denote the wall emissivity and surface unit normal vector, respectively. The symmetric conditions are applied on the symmetric plane at $x = 0$.

$$u = \frac{\partial v}{\partial x} = \frac{\partial T}{\partial x} = 0 \tag{14}$$

$$I(\mathbf{r}_{\text{sym}}, \hat{\mathbf{s}}) = I(\mathbf{r}_{\text{sym}}, \mathbf{s}') \quad \text{for} \quad |\hat{\mathbf{s}} \cdot \hat{\mathbf{n}}_{\text{sym}}| = |\hat{\mathbf{s}}' \cdot \hat{\mathbf{n}}_{\text{sym}}| \tag{15}$$

where $\hat{\mathbf{s}}$ and $\hat{\mathbf{s}}'$ represent the outgoing and incoming directions of the intensity and $\hat{\mathbf{n}}_{\text{sym}}$ is the unit vector normal to the symmetry plane.

Heat Transfer Rates

To investigate the characteristics of the heat transfer rate on the cylinder walls, the local Nusselt numbers at the inner and outer cylinder walls are defined as follows:

$$\text{Nu}_{\text{i}}^{C} = \frac{D_{\text{i}}}{\delta L} \left(-k \frac{\partial T}{\partial n} \right)_{\text{i}} \qquad \text{Nu}_{\text{o}}^{C} = \frac{D_{\text{o}}}{\delta L} \left(-k \frac{\partial T}{\partial n} \right)_{\text{o}} \tag{16}$$

$$\text{Nu}_{\text{i}}^{R} = \frac{\tau_{\text{o}} D_{\text{i}}}{4 N \delta L} \left(\int_{4\pi} I(\hat{\mathbf{s}}, \hat{\mathbf{n}}_{\text{w}}) \, d\Omega \right)_{\text{i}} \qquad \text{Nu}_{\text{o}}^{R} = \frac{\tau_{\text{o}} D_{\text{o}}}{4 N \delta L} \left(\int_{4\pi} I(\hat{\mathbf{s}}, \hat{\mathbf{n}}_{\text{w}}) \, d\Omega \right)_{\text{o}} \tag{17}$$

$$\text{Nu}_{\text{i}}^{T} = \text{Nu}_{\text{i}}^{C} + \text{Nu}_{\text{i}}^{R} \qquad \text{Nu}_{\text{o}}^{T} = \text{Nu}_{\text{o}}^{C} + \text{Nu}_{\text{o}}^{R} \tag{18}$$

Here n denotes the coordinate normal to the wall. While the superscripts C, R, and T represent the conductive, radiative, and total terms, the subscripts o and i denote the outer cold and inner hot walls, respectively, i.e., Nu^{T} represents the total local Nusselt number. Furthermore, in order to evaluate the average heat

transfer rate all along each cylinder wall, the following average Nusselt numbers are introduced:

$$\overline{\mathrm{Nu}}_{\mathrm{i}}^{C} = \frac{D_{\mathrm{i}}}{\delta L}\left(\frac{Q^{C}}{A}\right)_{\mathrm{i}} \qquad \overline{\mathrm{Nu}}_{\mathrm{o}}^{C} = \frac{D_{\mathrm{o}}}{\delta L}\left(\frac{Q^{C}}{A}\right)_{\mathrm{o}} \tag{19}$$

$$\overline{\mathrm{Nu}}_{\mathrm{i}}^{R} = \frac{\tau_{\mathrm{o}} D_{\mathrm{i}}}{4N\delta L}\left(\frac{Q^{R}}{A}\right)_{\mathrm{i}} \qquad \overline{\mathrm{Nu}}_{\mathrm{o}}^{R} = \frac{\tau_{\mathrm{o}} D_{\mathrm{o}}}{4N\delta L}\left(\frac{Q^{R}}{A}\right)_{\mathrm{o}} \tag{20}$$

$$\overline{\mathrm{Nu}}^{T} = \overline{\mathrm{Nu}}_{\mathrm{i}}^{C} + \overline{\mathrm{Nu}}_{\mathrm{i}}^{R} = |\overline{\mathrm{Nu}}_{\mathrm{o}}^{C} + \overline{\mathrm{Nu}}_{\mathrm{o}}^{R}| \tag{21}$$

Since the steady state is assumed in this study, the total average Nusselt number at the inner cylinder wall is equal to the absolute value of that at the outer cylinder wall, as in Eq. (21).

NUMERICAL ANALYSIS

Computational Procedure

To conduct a numerical analysis for the thermofluid dynamics fields, we adopt the compressible SIMPLER algorithm as developed by Karki [11]. It is known to maintain diagonal dominance of the pressure-correction equation when the covariant velocity components are used as dependent variables in the generalized body-fitted coordinate system. The convection terms are discretized using the QUICK finite difference scheme [12], while the central difference method is applied to the diffusion terms. In order to compute the radiation source term in the energy equation, the dimensionless linearized RTE is used here as proposed by Chai et al. [4]. A control volume surface intensity is evaluated from the nodal point value using a step spatial difference scheme [4] to ensure the positive intensity. For general irregular geometries, the control angles cannot be usually designed to match the physical boundaries exactly. In order to handle this problem, the radiative intensities at the boundary are managed by figuring out whether the intensity is incoming or outgoing, depending on the sign of directional weights, following Chai et al. [4].

After some preliminary calculations, the spatial and angular domains are discretized into 41×63 nonuniform control volumes in the ξ and η directions and 2×24 control angles with uniform $\Delta\phi$ and $\Delta\theta$ in the ϕ and θ directions, respectively. The typical spatial and angular control volumes are shown in Figure 2. The convergence criteria required for terminating computations are as follows:

$$\|\text{velocity}\|_2 < 10^{-3} \qquad \|T\|_2 < 10^{-4} \qquad \mathrm{Max}\left[|I_P^m - I_P^{m,\mathrm{old}}|/I_P^m\right] \leqslant 10^{-6} \tag{22}$$

Validation of Numerical Results

In order to validate our present numerical method for natural convection, a benchmark problem of the cylindrical annulus between horizontal concentric cylinders was solved and compared with the experimental results by Kuehn and

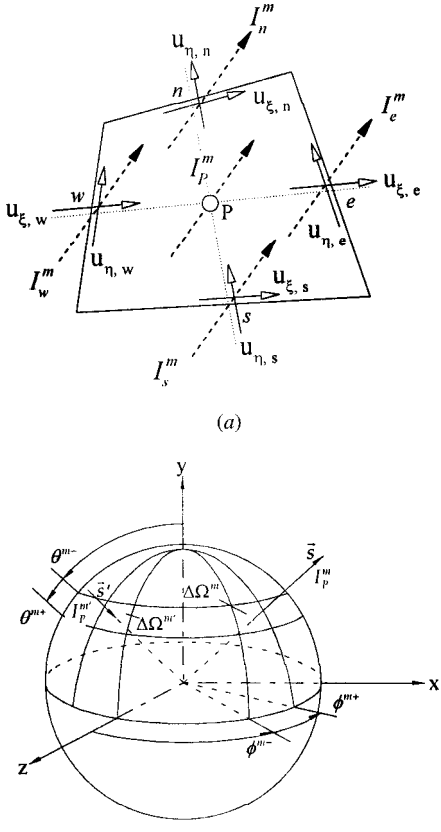

Figure 2. Representation of the spatial control volume and control angle: (*a*) staggered grid layout and example of typical radiation direction and (*b*) angular discretization used in the study.

Goldstein [6] for $\mathrm{Ra} = 4.8 \times 10^4$. Because of the small overheat ratio $\delta = 0.3$, the effect of radiation was excluded. A variation of the normalized local Nusselt number $\mathrm{Nu}/\mathrm{Nu}_C$ along the hot and cold surfaces, where Nu_C is the Nusselt number for pure conduction, is presented in Figure 3. The current results are shown to be in reasonably good agreement with the experimental data. In Figure 4 the numerical solutions of isotherms and streamlines for concentric and eccentric cylinders are plotted side-by-side with the experimentally obtained isotherms by Kuehn and Goldstein [7] for three eccentricities of $e_v/L = 0$, -0.623, and 0.652, for comparison. As with the previous case, the overheat ratio was 0.3 so that the effect of radiation could be safely neglected. As shown in the figure, the numerically obtained isotherms are consistent with the experimental contours.

The case with radiation effects is verified by considering a long cylindrical annulus filled with a homogeneous, absorbing-emitting medium. The calculation was implemented on a half domain by assigning symmetric conditions on the geometrically symmetric axis. The cylinder walls are assumed to be black and cold, and furthermore, the enclosed medium is held at a constant temperature T_g. Three absorption coefficients, namely, $\kappa = 0.1$, 1, and 5 m^{-1}, were considered. The

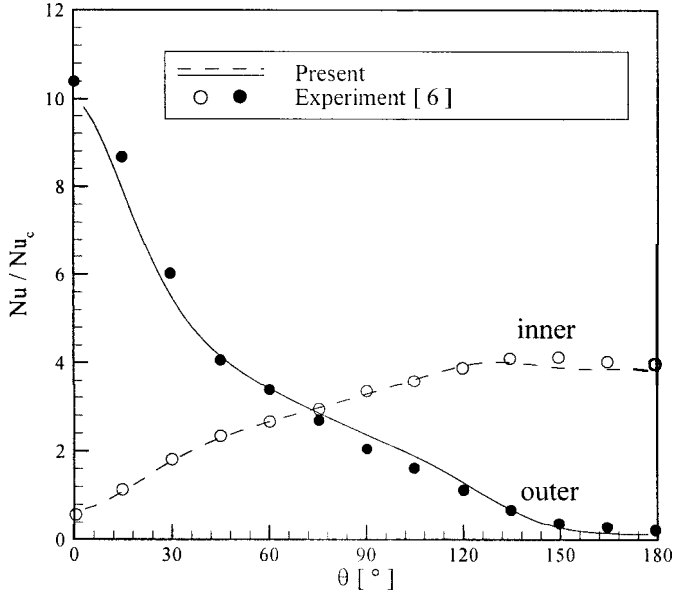

Figure 3. Normalized local Nusselt number validation around the cylinder for $e_y/L = 0$ and $\delta = 0.3$ at $\mathrm{Ra} = 4.8 \times 10^4$.

spatial and angular domains in the FVM consist of 15×23 uniform control volumes in the ξ and η directions and 2×24 control angles with uniform $\Delta\phi$ and $\Delta\theta$ in the ϕ and θ directions. With the DOM [13], recently developed for generalized body-fitted coordinate systems, the S_6 quadrature set was employed with the same spatial grids. In Figure 5 the calculated radiative heat fluxes in the radial direction are compared to the exact solutions obtained by Dua and Cheng [14]. It is found that the present results by FVM agree very well with the benchmark solutions.

RESULTS AND DISCUSSION

The results on the eccentric as well as concentric cylindrical annuli will be presented for an overheat ratio of unity with the radiation effects incorporated. In all the results presented here, the reference Prandtl and Rayleigh numbers are held at 0.685 and 1.5×10^4, respectively, while the fluid properties are estimated at the reference temperature 600 K. Whereas the cold outer wall temperature T_C is 300 K, the hot inner wall temperature T_H is 900 K. In the following, the results are rendered for three vertically eccentric positions of the inner cylinder with respect to the outer one with vertical eccentricity of $e_y/L = 0$, -0.623, and 0.652.

In Figures 6–8 the effects of N, a parameter measuring the relative effect of conduction to radiation, on the variations of isotherms and streamlines, are illustrated for three different vertical positions of the inner cylinder. Each figure consists of five cases; one for the baseline nonradiative case plus four for different values of N. The radiatively active medium in the enclosure is assumed to be

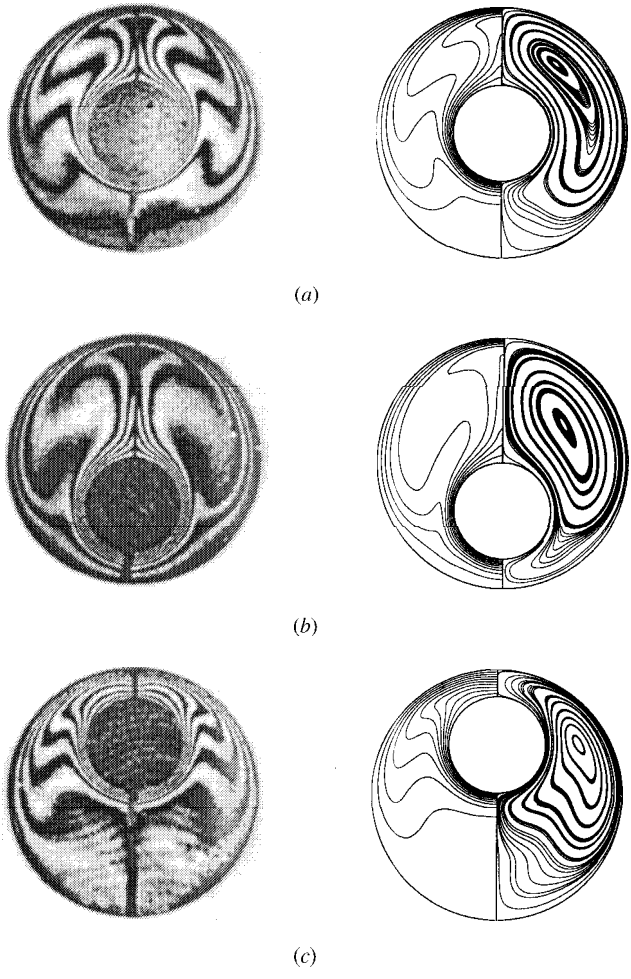

Figure 4. Comparison of experimental isotherms [7] with present calculated isotherms and streamlines for $\delta = 0.3$ and $\mathrm{Ra} = 4.8 \times 10^4$: (*a*) $e_v/L = 0$, (*b*) $e_v/L = -0.623$, and (*c*) $e_v/L = 0.652$.

nonscattering ($\omega_0 = 0$) with a constant optical thickness $\tau_0 = 0.3$ so that only absorption and emission of radiation occur inside. The inner and outer cylinder walls are assumed to be black. Scattering can, of course, easily be implemented in the current numerical procedure; however, since its effects can be inferred from the current nonscattering case, an additional calculation is not repeated here.

As N decreases, the radiation source term in the energy equation plays a more significant role, and the effect of radiation is augmented physically. For a smaller N the participating medium contained between the two cylinders can absorb more radiant energy and transform it into thermal energy, thereby increasing the overall medium temperature compared with the nonradiative case, as shown in the broadening isotherms in Figure 6. This is due to the so-called

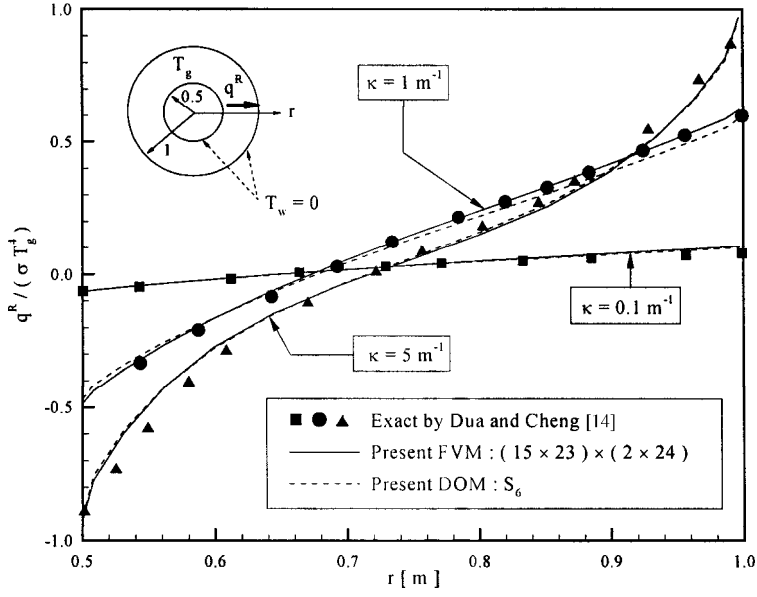

Figure 5. Validation of dimensionless radial heat flux along the radial direction for the isothermal absorbing-emitting medium.

far-reaching effect of the radiation. Consequently, once the medium participates in the absorption and emission of radiation, the medium temperature tends to be more uniform. Furthermore, as the participating medium attenuates the radiation more, a direct interaction of the inner hot wall with the outer cold wall, i.e., surface radiation, is reduced. This is clearly evidenced by observing a downward shift of the isotherm of unity closer to the outer cold cylindrical wall in Figure 6 for the concentric case as N decreases. This also causes the convective cell center to migrate downward. Similar trends are also observed in Figure 7 for the results with a positive eccentricity. In this case the convective motion is suppressed because of its thermally stable configuration; near the upper portion of the annulus the inner hot cylinder is facing upward toward the outer cold cylinder with a smaller distance apart. Accordingly, as shown in Table 2, the total average heat transfer from the hot inner cylinder is reduced for a fixed N when the inner cylinder is moved upward. This results in weaker convection near the lower part of the inner cylinder for the positive eccentric case. This fact can also be seen in Figure 9*c*, which represents a local total Nusselt number distribution at both walls along the polar angle. In Table 2, it is also shown that the total average Nusselt number increases as N decreases regardless of the eccentricity because the convective movement becomes more vigorous, especially for the positive eccentricity. Concurrently, a subsequent downward shift of the convective cell center is seen to be more obvious in Figure 7*e*.

When the inner cylinder is displaced downward, as shown in Figure 8, the location of the convective cell center barely changes. Moreover, compared to the previous two cases, N has an insignificant effect in the medium temperature

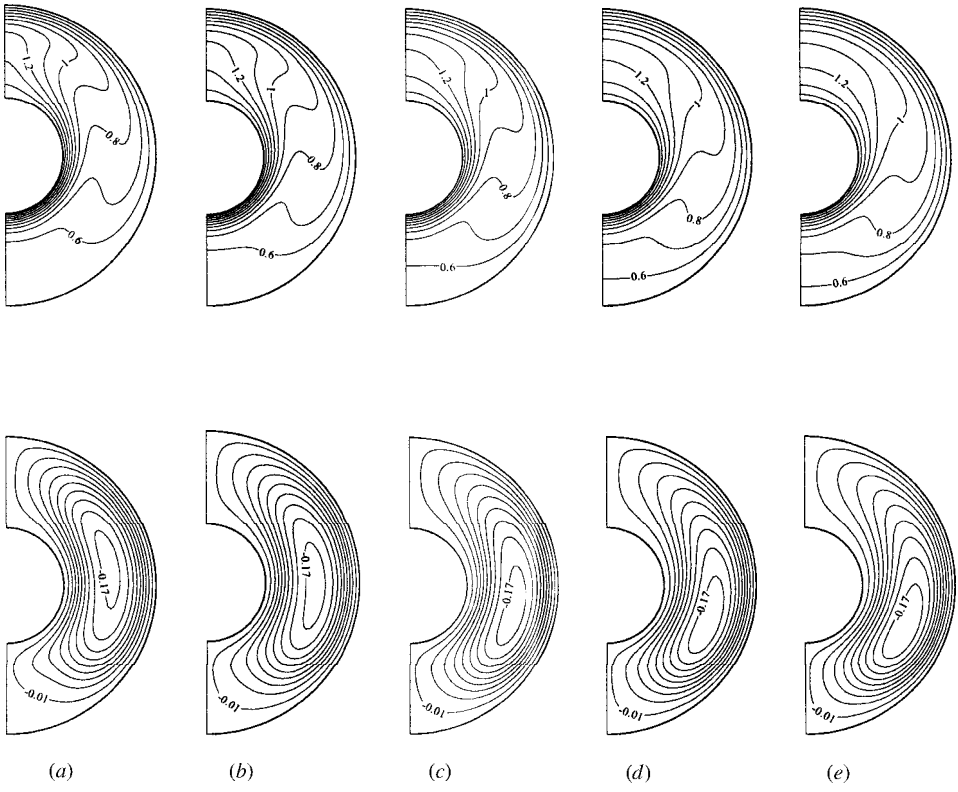

Figure 6. Isotherms (upper, $\Delta T = 0.1$) and streamlines (lower, $\Delta\Psi = 0.02$) in a concentric annulus ($e_y/L = 0$) for various conduction to radiation parameters N with $\mathrm{Ra} = 1.5 \times 10^4$, $\delta = 1$, $\tau_0 = 0.3$, $\omega_0 = 0$, and black boundaries: (*a*) without radiation, (*b*) $N = 0.1$, (*c*) $N = 0.05$, (*d*) $N = 0.03$, and (*e*) $N = 0.02$.

variation. This is derived from the fact that the thermofluid dynamics characteristics become buoyancy dominant. In other words, when the inner cylinder is located at a downward position, the internal buoyancy-induced flow becomes stronger, which in turn, results in higher heat transfer rate. This fact can also be deduced from Table 2. In Figure 8 a temperature inversion in isotherms over the upper section of the inner cylinder is more prominent because of the stronger convective motion.

In Figure 9 the conductive, radiative, and total Nusselt number variations around the inner and outer cylinder walls are depicted, depending on the eccentricity for a fixed value of the conduction to radiation parameter. The conductive wall heat flux directed into the outer cylinder is dominant over the upper region, especially for the positive eccentricity. The comparable result is shown over the lower region of the cylinder for the negative eccentricity. The present calculations are in qualitative agreement with the experimental data obtained by Kuehn and Goldstein [7] for different conditions.

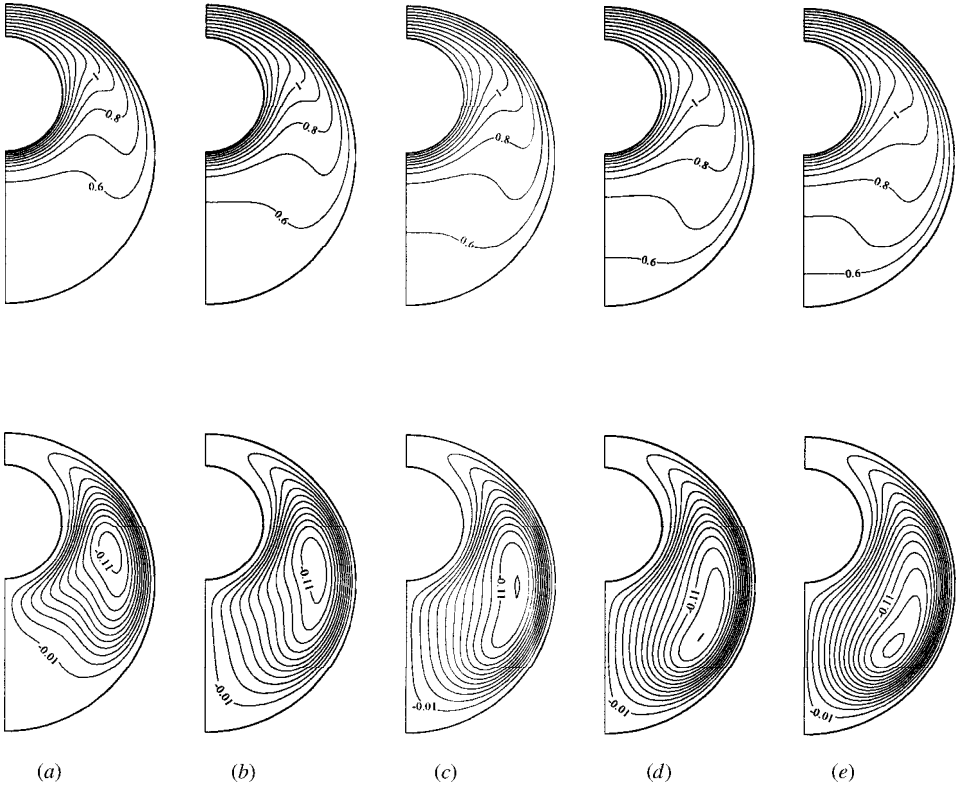

Figure 7. Isotherms (upper, $\Delta T = 0.1$) and streamlines (lower, $\Delta\Psi = 0.01$) in an eccentric annulus ($e_v / L = 0.652$) for various conduction to radiation parameters N with $\mathrm{Ra} = 1.5 \times 10^4$, $\delta = 1$, $\tau_0 = 0.3$, $\omega_0 = 0$, and black boundaries: (*a*) without radiation, (*b*) $N = 0.1$, (*c*) $N = 0.05$, (*d*) $N = 0.03$, and (*e*) $N = 0.02$.

The radiative Nusselt number in Figure 9*b* is significantly affected by the eccentricity with some general trends. The eccentricity is shown to influence the outer cylinder more significantly than the inner cylinder in radiative heat flux distribution. While the radiative heat flux from the inner cylinder is almost uniform over the polar angle, the radiative heat flux into the outer cylinder is seen to be the highest over the upper section and the lowest over the lowest section for the positive eccentricity. For the negative eccentricity this trend is reversed, as shown in the figure. Consequently, as far as the radiative heat flux is concerned, the outer cylinder is found to be significantly influenced by the location of the inner cylinder.

The distribution of the total local Nusselt number Nu^T around the polar angle is represented in Figure 9*c*. Since the radiative heat transfer is more dominant over the convective heat transfer, as seen in Figures 9*a* and 9*b*, a similar trend to that observed for the radiative Nusselt number is seen in Figure 9*c*. For the inner cylinder the total Nusselt number for the negative eccentricity attains highest values for most of the polar angle except for the upper section of the annulus.

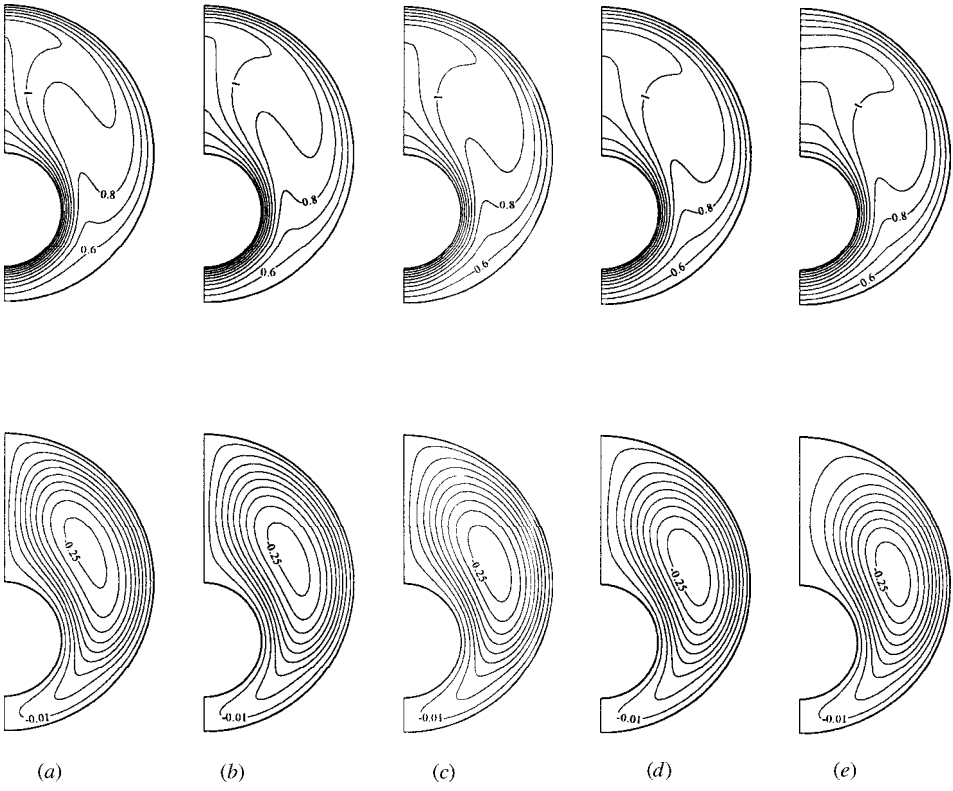

Figure 8. Isotherms (upper, $\Delta T = 0.1$) and streamlines (lower, $\Delta\Psi = 0.03$) in an eccentric annulus ($e_v/L = -0.623$) for various conduction to radiation parameters N with $\mathrm{Ra} = 1.5 \times 10^4$, $\delta = 1$, $\tau_0 = 0.3$, $\omega_0 = 0$, and black boundaries: (*a*) without radiation, (*b*) $N = 0.1$, (*c*) $N = 0.05$, (*d*) $N = 0.03$, and (*e*) $N = 0.02$.

When there exists a large temperature difference between two cylinders, it is known that the existence of a radiatively participating medium makes an apparent difference in fluid dynamics and thermal behavior. Combined with Table 2, the average value of the total Nusselt number is highest for the case with negative eccentricity and smallest for the case with positive eccentricity.

Table 2. Average total Nusselt number values

	e_v/L		
N	0.652	0	−0.623
0.1	8.538	8.989	9.579
0.05	12.768	13.059	13.860
0.03	18.452	18.628	19.563
0.02	25.625	25.676	26.638

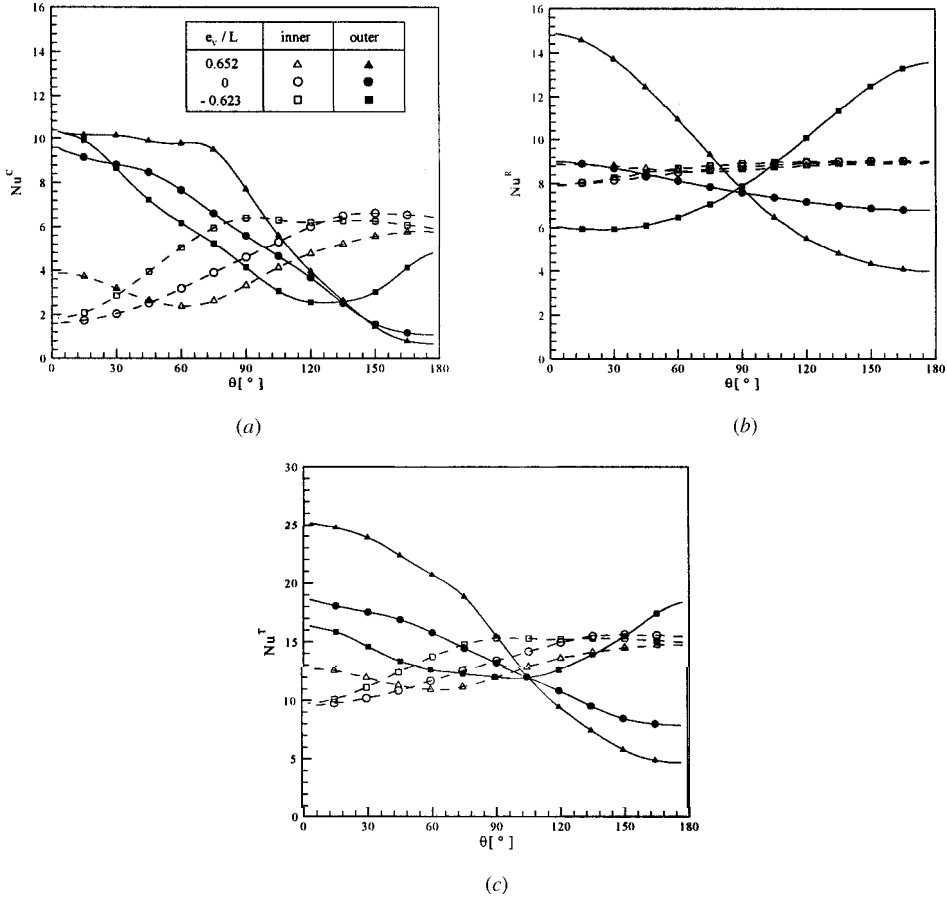

Figure 9. The effect of eccentricity on various Nusselt numbers for $N = 0.05$, $\mathrm{Ra} = 1.5 \times 10^4$, $\delta = 1$, $\tau_0 = 0.3$, $\omega_0 = 0$, and black boundaries: (*a*) Nu^C, (*b*) Nu^R, and (*c*) Nu^T.

CONCLUSIONS

A numerical investigation has been performed to examine the interaction between radiation and steady laminar natural convection in the cylindrical annuli filled with a gray gas. Radiation was found to play an important role in determining thermofluid dynamics behavior in natural convection induced by the hot inner cylinder under the large temperature difference. The main results are as follows.

1. As N decreases, the medium temperature increases overall and becomes more uniform due to the far-reaching effect of radiation.
2. Regarding the heat flux distribution around the cylinder, the eccentricity affects the outer cylinder more significantly than the inner cylinder.
3. Regardless of eccentricity, the total average Nusselt number usually increases as N decreases.

4. The average value of the total Nusselt number around the outer cylinder attains the highest value for the case with negative eccentricity, which is accompanied by the strong convective motion due to buoyancy.

REFERENCES

1. T. Y. Kim and S. W. Baek, Analysis of Combined Conductive and Radiative Heat Transfer in a Two-Dimensional Rectangular Enclosure Using the Discrete Ordinates Method, *Int. J. Heat Mass Transfer*, vol. 34, pp. 2265–2273, 1991.
2. C. Y. Han and S. W. Baek, Radiative Ignition of Volatile Gases on a Vertical Fuel Plate, *Combust. Sci. Technol.*, vol. 109, pp. 309–325, 1995.
3. E. H. Chui and G. D. Raithby, Computation of Radiant Heat Transfer on a Nonorthogonal Mesh Using Finite-Volume Method, *Numer. Heat Transfer, Part B*, vol. 23, pp. 269–288, 1993.
4. J. C. Chai, H. S. Lee, and S. V. Patankar, Finite-Volume Method for Radiation Heat Transfer, *J. Thermophys.*, vol. 8, pp. 419–425, 1994.
5. M. Y. Kim and S. W. Baek, Numerical Analysis of Conduction, Convection and Radiation in a Gradually Expanding Channel, *Numer. Heat Transfer, Part A*, vol. 29, pp. 725–740, 1996.
6. T. H. Kuehn and R. J. Goldstein, An Experimental and Theoretical Study of Natural Convection in the Annulus Between Horizontal Concentric Cylinders, *J. Fluid Mech.*, vol. 74, no. 4, pp. 695–719, 1976.
7. T. H. Kuehn and R. J. Goldstein, An Experimental Study of Natural Convection Heat Transfer in Concentric and Eccentric Horizontal Cylindrical Annuli, *J. Heat Transfer*, vol. 100, pp. 635–640, 1978.
8. C. H. Cho, K. S. Chang, and K. H. Park, Numerical Simulation of Natural Convection in Concentric and Eccentric Horizontal Cylindrical Annuli, *J. Heat Transfer*, vol. 104, pp. 624–630, 1982.
9. G. Lauriat, Combined Radiation-Convection in Gray Fluids Enclosed in Vertical Cavities, *J. Heat Transfer*, vol. 104, pp. 609–615, 1982.
10. T. Fusegi and B. Farouk, Laminar and Turbulent Natural Convection-Radiation Interactions in a Square Enclosure Filled with a Nongray Gas, *Numer. Heat Transfer, Part A*, vol. 15, pp. 303–322, 1989.
11. K. C. Karki and S. V. Patankar, Pressure-Based Calculation Procedure for Viscous Flows at All Speeds in Arbitrary Configurations, *AIAA J.*, vol. 27, no. 9, pp. 1167–1174, 1989.
12. S. Thakur and W. Shyy, Some Implementational issues of Convection Schemes for Finite-Volume Formulations, *Numer. Heat Transfer, Part B*, vol. 24, pp. 31–55, 1993.
13. J. Liu, H. M. Shang, Y. S. Chen, and T. S. Wang, Prediction of Radiative Transfer in General Body-Fitted Coordinates, *Numer. Heat Transfer, Part B*, vol. 31, pp. 423–439, 1997.
14. S. S. Dua and P. Cheng, Multi-Dimensional Radiative Transfer in Non-Isothermal Cylindrical Media with Non-Isothermal Bounding Walls, *Int. J. Heat Mass Transfer*, vol. 18, pp. 245–259, 1975.